Open Access

Recent Progress in Materials

LIDSEN Publishing Inc.

Research Article

Electrochemical Atomic Layer Epitaxy Deposition of Ultrathin SnTe Films

Taise M. Manhabosco [1,*], Shaul Aloni [2], Tevye R. Kuykendall [2], Sara M. Manhabosco [3], Ana Bárbara Batista [1], Jaqueline S. Soares [1], Ana Paula M. Barboza [1], Alan. B. de Oliveira [1], Ronaldo J. C. Batista [1], Jeffrey J. Urban [2]

1. Departamento de Física, Universidade Federal de Ouro Preto, Campus Universitário Morro do Cruzeiro ICEB/DEFIS, 35400-000, Ouro Preto, Minas Gerais, Brazil; E-Mails: taise@ufop.edu.br; anabc.batista@gmail.com; jssoares@iceb.ufop.br; ana.paula@iceb.ufop.br; deoliveira.alanbarros@gmail.com; batista.rjc@iceb.ufop.br
2. The Molecular Foundry, Lawrence Berkeley National Laboratory, Berkeley, California 94720, USA; E-Mails: saloni@lbl.gov; TRKuykendall@lbl.gov; jjurban@lbl.gov
3. Laboratório de Metrologia, Universidade Federal do Rio Grande, Campus Carreiros, Av. Itália, km 8, 96203-900, Rio Grande, Rio Grande do Sul, Brazil; E-Mail: saramm@furg.br

* **Correspondence:** Taise M. Manhabosco; E-Mail: taise@ufop.edu.br

Academic Editor: Hossein Hosseinkhani

Recent Progress in Materials
2019, volume 1, issue 4
doi:10.21926/rpm.1904005

Received: September 06, 2019
Accepted: October 21, 2019
Published: October 29, 2019

Abstract

Tin telluride (SnTe) ultrathin films were deposited electrochemically on polycrystalline and monocrystalline gold substrates using the electrochemical atomic layer epitaxy (ECALE) method. The electrochemical behaviors of Sn and Te were studied systematically by means of cyclic voltammetry. Cyclic voltammetry curves for Sn displayed a broad peak in the region between -0.15 V and -0.35 V, which was related to the under-potential deposition (UPD), while the curves for Te displayed a peak at 0.3 V for Te UPD. X-ray photoelectron spectroscopy (XPS), X-ray diffraction (XRD), Raman spectroscopy, and scanning electron microscopy (SEM) were employed for the characterization of the ultrathin SnTe films. XRD and Raman spectroscopy confirmed the deposition of a single SnTe phase, while SEM revealed that the deposits were composed of nanocrystallites.

Keywords
SnTe; electrochemical atomic layer epitaxy deposition; under-potential deposition; thin films

1. Introduction

The importance of tin telluride (SnTe) films has been increasing over the years, owing to its unique transport properties which enable the study of new physical phenomena. For instance, SnTe films are topological insulators, that is, they behave as insulators when in bulk although with protected conducting surface states [1, 2]. In addition, semiconductors such as SnTe are among the most popular areas of study in the field of optoelectronic science. Among the different possible applications of SnTe, including microeletronics, batteries, and photovoltaics, SnTe also serves as a thermoelectric material to be used in thermoelectrical devices such as thermoelectric generators which have been applied successfully in aerospace, military, and automotive industry [3, 4].

In general, SnTe films are produced by means of spark plasma sintering, magnetron sputtering, pulsed laser deposition, molecular-beam epitaxy (MBE), etc. [5-8]. All these methods rely on the availability of precursors, vacuum requisitions, and stability at high temperatures, imposing restrictions on these methods and rendering them expensive to apply. On the other hand, electrodeposition, an old although well-established technique, is relatively simple, inexpensive, and is often performed at room temperature. This technique has been used extensively to deposit a large variety of compound semiconductors and metals with good quality and performance.

In 2011, Sisman and Öz first reported the production of SnTe thin films using over potential deposition (OPD) [9]. OPD occurs at more negative potentials rather than at the Nernst potential (equilibrium potential). This technique is dependent on the electrode potential (overpotential), on the concentration of the electroactive species, and on the deposit-substrate and deposit-deposit interactions. In contrast, under potential deposition (UPD) occurs at more positive potentials rather than at Nernst potential, and is referred to as a surface-limited phenomenon in which the electrode surface is partially or completely covered by a deposit. Gregory and Stickney [10] developed a method for the electrochemical deposition of compound semiconductors, which was referred to as the “electrochemical atomic layer epitaxy” (ECALE) method. ECALE is a variation of UPD, in which contrary to the standard electrochemical deposition, a compound layer is formed by depositing an atomically thin layer of one element at a time.

The ECALE method has been employed to deposit a variety of semiconductors, such as CdTe, Bi_2Se_3, CdSe, CdS, $Ge_xSb_yTe_z$, etc. [6, 11-16]. According to our knowledge, deposition of SnTe thin films using the ECALE method has not been reported so far. In the present work, deposition of SnTe thin films using the ECALE method was studied systematically by means of cyclic voltammetry, and the obtained films were characterized using X-ray photoelectron spectroscopy (XPS), X-ray diffraction, Raman spectroscopy, and scanning electron microscopy (SEM).

2. Materials and Methods

The substrates used in the present study were polycrystalline gold deposited on silicon with a 5 nm chromium interlayer, and monocrystalline gold (111) deposited on quartz. Prior to each electrochemical experiment, cycles of oxidation and reduction -were performed (between −0.35 V and 1.5 V) in 1 M H_2SO_4 solution in order to clean the gold surface. At least eight cycles were performed prior to each experiment.

The electrochemical experiments were performed in a thin-layer electrochemical cell having a volume of 93.6 μL. The employed counter electrode consisted of a platinum mesh, and an Ag/AgCl electrode (eDAQ) was employed as the reference electrode.

Sn solutions were prepared using 0.5 mM $SnCl_2$ and 0.1 M $HClO_4$, and the pH of the solution was maintained at 1.38. Te solutions were prepared using 0.5 mM TeO_2 and 0.1 M $HClO_4$, and the pH of the solution was maintained at 1.44. The supporting electrolyte was prepared using 1 M $NaClO_4$, at pH = 2.7. The solutions of $SnCl_2$, $HClO_4$, TeO_2, and $NaClO_4$ (Sigma-Aldrich; purity > 99.99%) were prepared in ultrapure water (18 MΩ.cm), and purged with N_2 prior to each electrochemical experiment. The Sn solutions were freshly prepared prior to each experiment in order to avoid solution oxidation. The electrode was always rinsed with the supporting electrolyte prior to Te or Sn deposition, in order to clean the gold surface and the electrochemical cell to avoid codeposition.

Cyclic voltammetry (CV) of Sn and Te on gold electrode was performed at a scan rate of 10 mV/s in order to obtain the UPD peak for both the elements. The deposition of the SnTe films was accomplished by depositing alternating Te and Sn monolayers. After each electrodeposition step, the obtained material was rinsed with the supporting electrolyte to remove the deposition ions from the solution. All the experiments were performed at least in triplicate to ensure reproducibility and repeatability with errors smaller than 10%. XPS of the deposits was analyzed using a Phi 5400 ESCA electron spectrometer equipped with an Mg K X-ray source. The XRD patterns were obtained on a Bruker D8-Discover X-ray diffractometer, which was equipped with a GADDS area detector and was operated at 40 kV and 20 mA at the wavelength of Cu Kα 1.5406 Å. The Raman spectra were recorded on Horiba Jobin Yvon LabRAM ARAMIS automated scanning confocal Raman microscope using laser excitation at 532 nm. SEM was employed to display the morphology of the deposits.

3. Results and Discussion

3.1 Cyclic Voltammetry

Cyclic voltammetry experiments were performed using gold polycrystalline as a substrate. Cyclic voltammograms for the Au electrode in the solutions composed of $SnCl_2$ and $HClO_4$ are depicted in Figure 1(a) and 1 (b). When the potential was scanned from 0.4 V to -0.4 V, as depicted in Figure 1 (a), a broad cathodic peak C1 appeared between -0.15 V and -0.35 V, which was assigned to the UPD of Sn on Au [9, 17]. In the reverse scan, a broad anodic peak (A1) appeared between 0 V and 0.2 V, which corresponded to the stripping of the monolayer deposited at UPD [9]. It is important to mention that UPD process is highly influenced by the surface state of the substrate, which plays a critical role in the initial stages of metal deposition, causing the reduction/oxidation potential to differ from the equilibrium potential of the involved species [18]. Scanning further to -0.47 V, as depicted in Figure 1 (b), revealed two new cathodic peaks, namely,

C2 and C3. C2, located at -0.44 V, corresponded to the multi-atomic deposition of Sn layers [9, 19], while C3, located at -0.47 V, corresponded to the deposition of the Sn bulk in the overpotential deposition (OPD) region [9]. The anodic peaks A2 and A3 corresponded to the dissolution of the multilayered Sn and the Sn bulk, respectively [9]. Two minor peaks were observed at approximately -0.4 V and -0.33 V in the anodic scan, which were also presented in the cyclic voltammograms reported by Sisman and ÖZ for the same element [9]. The authors [9] did not mention the origin of these peaks, although it is believed that the presence of these two peaks could have been due to Sn bulk material that was not dissolved by the A3 process (i.e., Sn bulk dissolution). This implied that the residual bulk-like material in contact with the multilayered Sn could have higher biding energy than that of the bulk, requiring higher potentials to be dissolved.

The cyclic voltammograms for the Au electrode in a mix of TeO_2 and $HClO_4$ are depicted in Figure 2 (a) and 2 (b). Figure 2(a) depicts a cathodic peak C1 at 0.3 V, which corresponded to the UPD of Te monolayer on Au. The broad cathodic peak C2 observed between -0.15 V and -0.3 V was assigned to the deposition of Te bulk. In the reverse scan, the peak A2 was assigned to the stripping of Te bulk, and the peak A1 was associated with the UPD stripping of Te. A similar curve for Te on Au was reported by Gregory and Stickney [10]. Figure 2(b) illustrates that the hydrogen evolution and reduction of Te to H_2Te reached the maximum value among the current values. The excess conversion of H^+ to H_2Te and H_2 at potentials higher than -0.8 V is an uncontrolled process that is responsible for the observed noise in the CV.

It is worth mentioning that besides the conventional UPD deposition, there is another way to deposit Te UPD on Au [10]. In this method, a complete TeO_2 aliquot is deposited at -0.3 V, with a subsequent reduction of the excess Te (Te bulk) to H_2Te at -0.85 V, followed by the rinsing away of H_2Te with pure electrolyte. The Te bulk would be dissolved at -0.85 V, leaving a monolayer of Te atoms.

The initial deposition of one element on a substrate (in this case, gold) is different from the subsequent deposition as the latter does not occur on the initial substrate anymore [20]. However, the cyclic voltammograms for the Te-covered Au electrode in $SnCl_2$ (Figure 3) exhibited similarities to the CVs of bare Au electrode in $SnCl_2$ and in TeO_2 solutions (Figure 1 and 2, respectively). It is clearly visible that the UPD feature (C1) occurred at the same potential in both Figure 1 and Figure 2. Moreover, the reverse scan depicted in Figure 3 illustrates the stripping of Sn (A1 peak) and Te (A2 peak) monolayers, which are also present in Figure 1 and Figure 2, respectively. Such similarities indicated that the subsequent deposition of Sn on the Te-covered Au electrode occurred preferentially on the remnant open gold sites rather than on the Te-covered sites, a phenomenon reported in previous studies as well [11, 20].

The cyclic voltammetry experiments were also performed using single-crystalline gold as substrate. It was observed that there were changes in the position of the reduction peak relative to the depositions on the polycrystalline Au substrate, which was in agreement with the findings reported by Mendoza-Huizar et al. [21].

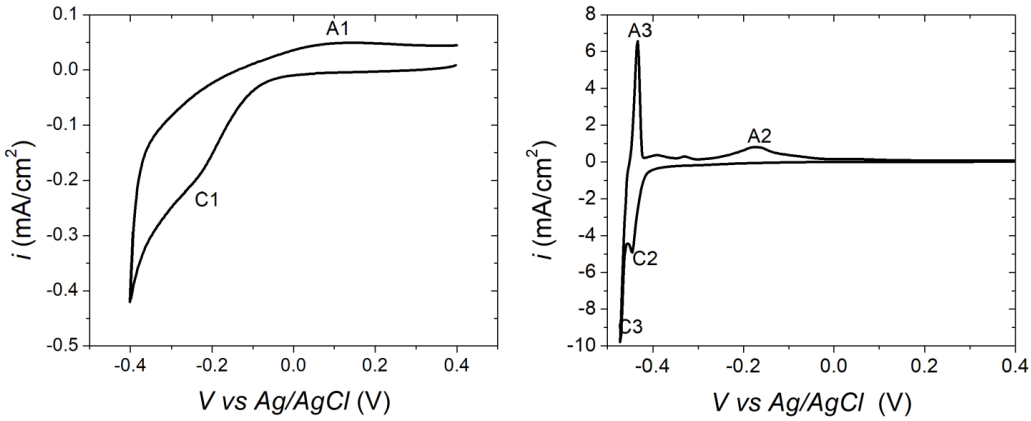

Figure 1 Cyclic voltammograms for Au polycrystalline electrode in $SnCl_2$ and $HClO_4$ solution (a) Scanning range window: from 0.4 V to -0.4 V (b) Scanning range window: from 0.4 V to -0.47 V. The scanning rate is 10 mV/s.

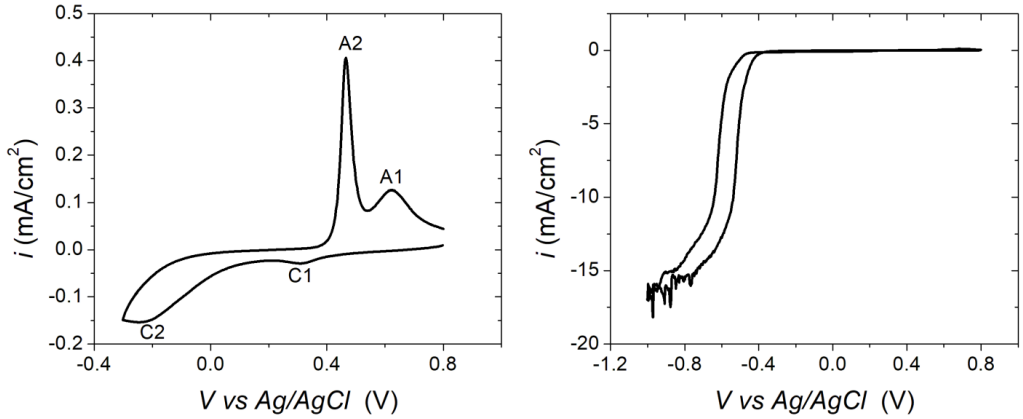

Figure 2 Cyclic voltammograms for Au polycrystalline electrode in TeO_2 and $HClO_4$ solution (a) Scanning range window: from 0.8 V to -0.3 V (b) Scanning range window: from 0.8 V to -1.0 V. The scanning rate is 10 mV/s.

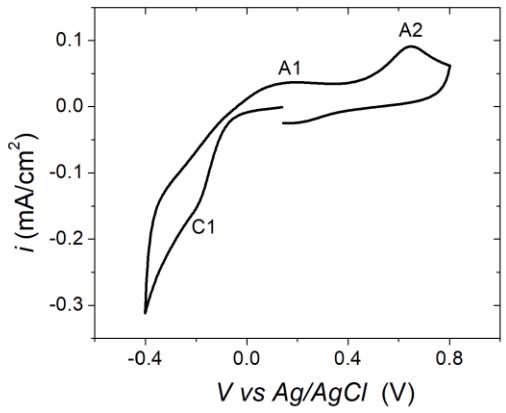

Figure 3 Cyclic voltammograms for Te-covered Au polycrystalline electrode in $SnCl_2$ and $HClO_4$ solution at a scanning rate of 10 mV/s.

3.2 Alternating Sn-Te Multilayer Deposition

ECALE involves sequential electrochemical deposition of elements to form nanofilms of a composite material. In the present study, deposition of Sn was performed using UPD, by applying a potential of -0.3 V for 5 sec. The deposition of Te could not be performed at 0.3 V because the stripping peak of Sn was observed between 0 V and 0.2 V. The only way of depositing a monolayer of Te was to deposit a bulk amount of Te at -0.3 V for 60 sec, followed by a subsequent reduction of excess Te at -0.85 V for 5 sec. The Te reduction was performed in a supporting electrolyte (1 M $NaClO_4$) and in this process, the excess Te was reduced to soluble telluride species (H_2Te) and was rinsed away [12, 21].

In order to obtain alternating Sn and Te layers, the process described above was repeated several times. At each cycle, first a Te layer was deposited, followed by a layer of Sn, resulting in the following sequence: Au> Te> Sn> Te> Sn>.... Amperometric *i* vs. *t* curves for the alternating Sn and Te layers deposition are depicted in Figure 4. Panel (a) depicts the current densities during the UPD of Sn layers at the 1st, 10th, and 20th cycles. A decrease in the current densities with an increasing number of cycles was observed, which has been reported previously by other authors as well [22, 23]. This decrease reflected the fact that the physico-chemical characteristics of the substrate changed as the number of the deposited Sn-Te layers increased, that is, at each cycle, the effects exerted by the polycrystalline gold present below the Sn-Te layers on the Sn deposition diminish [22, 23]. In case of Te deposition process, depicted in Figure 4 (b), bulk was deposited at each cycle; therefore, the substrate may be strongly affecting the current densities only at the beginning of the deposition process. Nevertheless, it is visible in Figure 4 (b) that there was a persistent increase in the current densities with increasing number of cycles. Such an increase in the current densities at over potential deposition (OPD) might be due to the increasing surface area of the deposition nuclei [24].

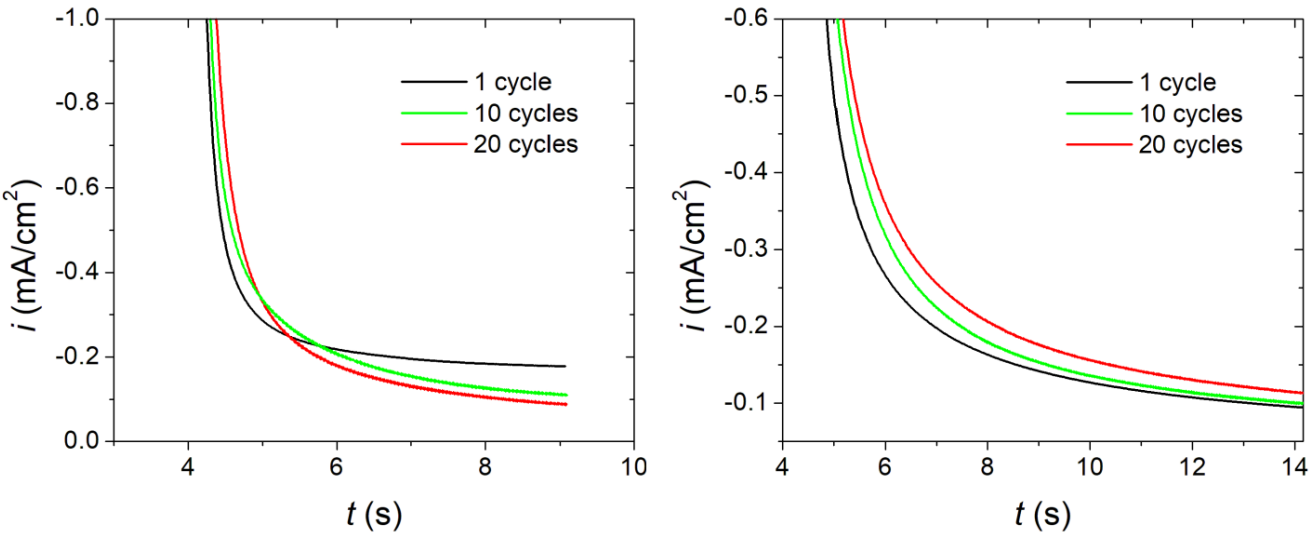

Figure 4 Amperometric *i vs. t* curves for Sn (a) and Te (b) at 1st, 10th and 20th cycles. Applied potentials for Sn and Te are -0.3 V *vs* Ag/AgCl. Each cycle corresponds to sequential deposition of Te and Sn deposits.

3.3 SnTe Characterization

Figure 5 depicts the XPS spectra of the prepared twenty layers of Sn-Te compound. All the peaks identified in the spectra were attributed to Sn, Te, C, and O. The presence of oxygen was attributed to the oxidation of the deposit, while the presence of carbon was attributed to atmospheric exposure. An XPS spectrum covering the Sn3d core-level energy-range is depicted in Figure 5 (b). The peaks at 487 eV and 495.5 eV corresponded to the binding energies of $Sn3d_{5/2}$ and $Sn3d_{3/2}$, respectively, which were close to the values reported previously in the literature [25]. An XPS spectrum covering the Te3d core-level has been depicted in Figure 5 (c). The peaks at 573 eV and 583.7 eV corresponded to the binding energies of $Te3d_{5/2}$ and $Te3d_{3/2}$, respectively, for elemental tellurium [9]. The peaks at 576 eV and 587.3 eV could be assigned to $Te3d_{5/2}$ and $Ted_{3/2}$, for TeO_2 [26].

Figure 6 (a) and 6 (b) depict the Raman spectra of thirty-layer SnTe films deposited on polycrystalline Au and bulk SnTe composite, respectively. The spectrum for the SnTe thin film exhibited the typical peaks of crystalline SnTe [27]. A shift in the Raman peaks could be observed for the SnTe thin film in comparison to the bulk SnTe composite, which might have occurred due to nanoscale size effects [28, 29].

The XRD pattern obtained for the sample containing thirty layers of SnTe film deposited on polycrystalline Au has been depicted in Figure 7. The XRD pattern of the sample was indexed as a pure cubic phase, which was quite close to the values reported previously in the literature (JSPDS No 46-1210). Five diffraction peaks related to the SnTe phase were observed, and were identified as (200), (220), (222), (400), and (420). The diffraction peaks observed at 38.15° (111) and 44.35° (200) were due to the growth on the Au polycrystalline substrate. Subsequently, the deposited films were crystallized in the preferential directions along the (200) and (222) planes, which suggested an epitaxial growth, as expected with the use of the ECALE technique. Epitaxial growth is highly influenced by the UPD deposition as the UPD process is a surface limited process that allows the monolayer that is being deposited to copy the crystalline structure of the substrate [10, 30]. Despite the XPS results in its favor, no peaks for elemental Te or Sn were observed in the XRD pattern, suggesting that the amounts of these elements were below the detection threshold. In addition, no oxide was detected, probably because the oxide layer deposited over the surface was quite thin.

Figure 8 displays the SEM image of ten layers of SnTe film deposited on monocrystalline Au. It is possible to view the border between the covered gold substrate and the bare substrate. The morphology of the films revealed that the surface was covered by small SnTe particles (light gray in color), with a grain size of approximately 20-30 nm, possibly implying a certain 3D growth [13, 31]. The presence of nuclei may be due to the Te OPD deposition process, which according to the Scharifker and Hills model [32] results in the formation of 3D nuclei [31]. The Te nuclei were subsequently dissolved to form monolayers.

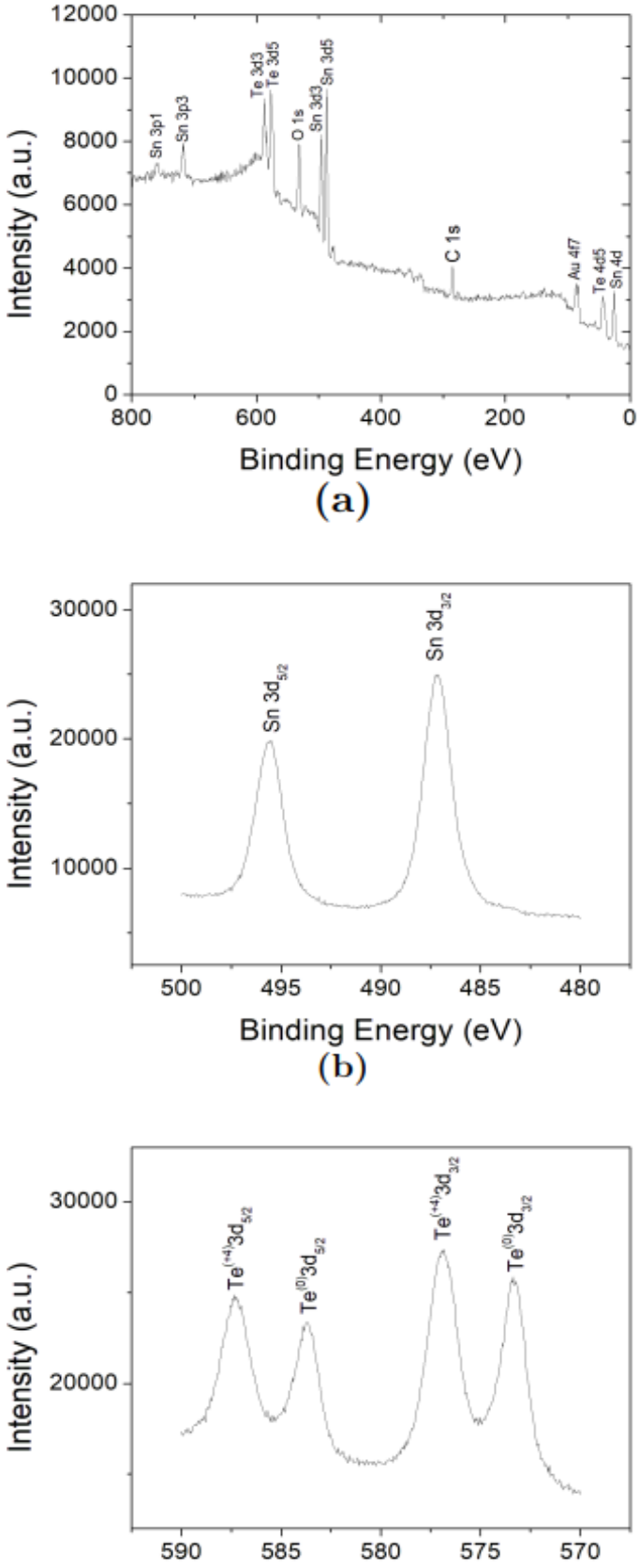

Figure 5 The XPS core level spectra of the as-prepared twenty layers of Sn-Te compound.

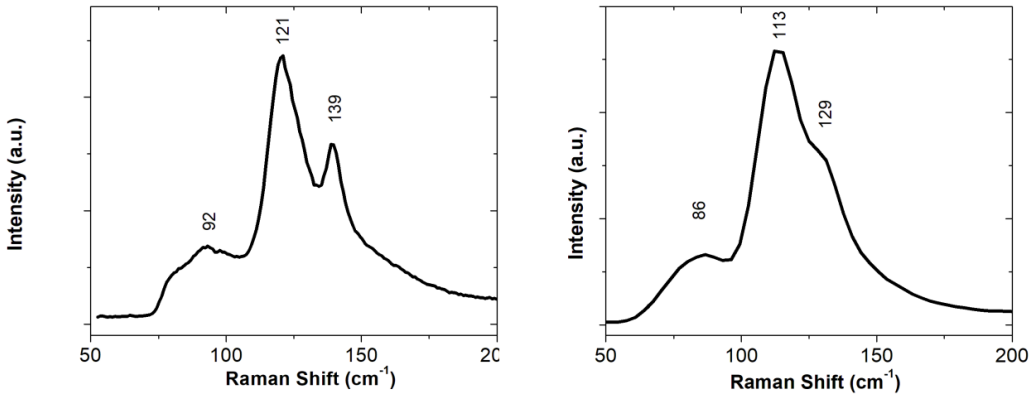

Figure 6 Raman spectra of SnTe (a) thin films and (b) bulk SnTe composite.

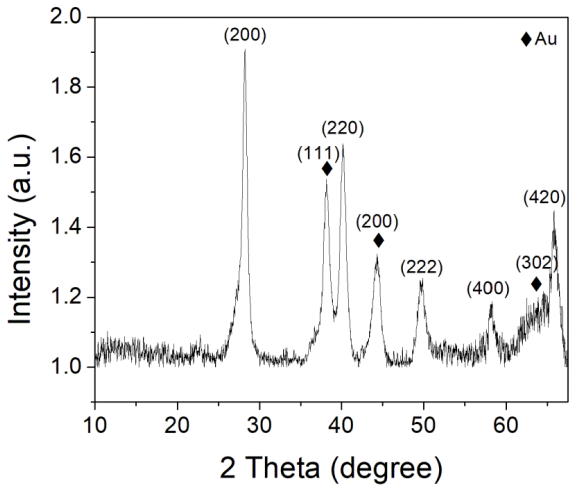

Figure 7 X-ray diffraction pattern of as-deposited SnTe thin films.

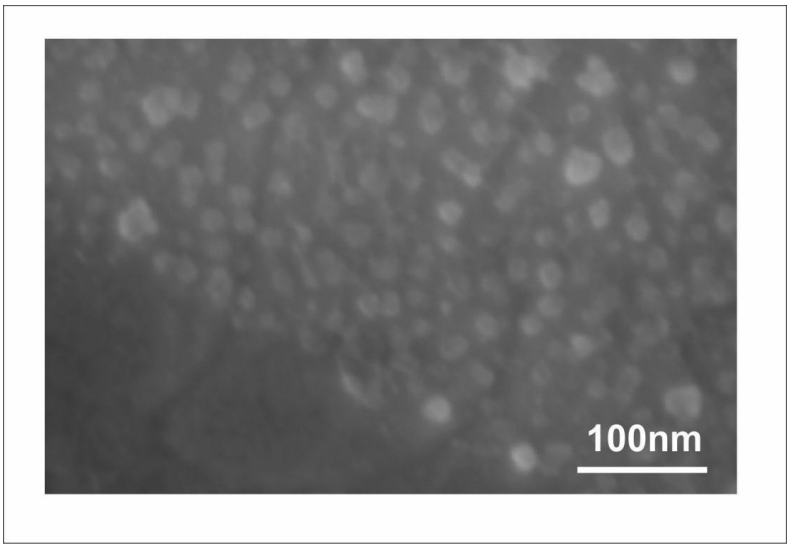

Figure 8 SEM image of ten layers SnTe thin films prepared by ECALE on monocrystalline gold substrate. Light gray color indicates the SnTe islands while dark gray color refers to the gold substrate.

4. Conclusions

SnTe films were successfully deposited on the gold electrode using the ECALE method. Electrochemical aspects of the Te and Sn depositions were characterized by means of cyclic voltammetry and chronoamperometry. The Raman measurement of the deposited films exhibited two main peaks which were characteristic of SnTe compound. The XRD analysis revealed that the deposit was single phase SnTe, with no evidence of elemental Sn or Te. The SEM images appeared to depict that the SnTe deposit was comprised of nanocrystalline particles.

Acknowledgments

The authors would like to thanks CNPq, CAPES and FAPEMIG agency for the financial support. Work at the Molecular Foundry was supported by the Office of Science, Office of Basic Energy Sciences of the U.S. Department of Energy under Contract No. DE-AC02-05CH11231.

Author Contributions

Taise M. Manhabosco – The author made cyclic voltammetry experiments and wrote the paper together with Alan. B. de Oliveira and Ronaldo J. C. Batista.

Jeffrey J. Urban - The author is the head of the project. He proposed and supervised the work.

Shaul Aloni – Dr. Aloni performed SEM experiments and helped with the development of the project.

Tevye R. Kuykendall and Jaqueline S. Soares performed Raman measurements and helped to interpret the results.

Sara M. Manhabosco and Ana Bárbara Batista redo the cyclic voltammetry experiments to ensure reproductibility.

Ana Paula M. Barboza- She helped with the identification of SnTe phase through X ray measurements.

Competing Interests

The authors have declared that no competing interests exist.

References

1. Zhang X, Zhang H, Wang J, Felser C, Zhang SC. Actinide topological insulator materials with strong interaction. Science. 2012; 335: 1464-1466.
2. Berchenko N, Vitchev R, Trzyna M, Wojnarowska-Nowak R, Szczerbakow A, Badyla A, et al. Surface oxidation of SnTe topological crystalline insulator. Appl Surf Sci. 2018; 452: 134-140.
3. Xu S, Zhu W, Zhao H, Xu L, Sheng P, Zhao G, et al. Enhanced thermoelectric performance of SnTe thin film through designing oriented nanopillar structure. J Alloys Compouds. 2018; 737: 167-173.
4. Wang X, Wang H, Su W, Zhai J, Wang T, Chen T, et al. Optimization of the performance of the SnTe uni-leg thermoelectric module via metallized layers. Ren Energy. 2019; 131: 606-616.

5. Teghil R, Guidoni AG, Mele A, Piccirillo S, Coreno M, Marotta V, et al. Pulsed laser induced ablation applied to epitaxial growth of semiconductor materials: Selenides and tellurides plume analysis. Surf Interface Anal. 1994; 22: 181-185.
6. Wu J, He J, Han MK, Sootsman JR, Girard S, Arachchige IU, et al. Electron-beam activated thermal sputtering of thermoelectric materials. J Appl Phys. 2011; 110: 044325.
7. Zayachuk DM, Slynko VE, Csik A. Peculiar properties of preferential sputtering of PbTe, SnTe, and GeTe by Ar^+ ion plasma. Mater Sci Semicond Proc. 2018; 88: 103-108.
8. Wang X, Wang H, Su W, Zhai J, Wang T, Chen T, et al. Optimization of the performance of the SnTe uni-leg thermoelectric module via metallized layers. Ren Energy. 2019; 131: 606-616.
9. Sisman I, Öz H. Preparation of SnTe thin films on Au (1 1 1) by electrodeposition route. Electrochim Acta. 2011; 56: 4889-4894.
10. Gregory BW, Stickney JL. Electrochemical atomic layer epitaxy (ECALE). J Electroanal Chem. 1991; 300: 543-561.
11. Foresti ML, Pezzatini G, Cavallini M, Aloisi G, Innocenti M, Guidelli R. Electrochemical atomic layer epitaxy deposition of CdS on Ag(111): An electrochemical and STM investigation. J Phys Chem B. 1998; 102: 7413-7420.
12. Mathe MK, Cox SM, Flowers BH, Vaidyanathan R, Pham L, Srisook N, et al. Deposition of CdSe by EC-ALE. J Cryst Growth. 2004; 271: 55-64.
13. Muthuvel M, Stickney JL. CdTe electrodeposition on InP(100) via electrochemical atomic layer epitaxy (EC-ALE): Studies using UHV-EC. Langmuir. 2006; 22: 5504-5508.
14. Xiao C, Yang J, Zhu W, Peng J, Zhang J. Electrodeposition and characterization of Bi2Se3 thin films by electrochemical atomic layer epitaxy (ECALE). Electrochim Acta. 2009; 54: 6821-6826.
15. Liang X, Jayaraju N, Thambidurai C, Zhang Q, Stickney JL. Controlled electrochemical formation of $Ge_xSb_yTe_z$ using atomic layer deposition (ALD). 2011; Chem Mater 23: 1742-1752.
16. Giurlani W, Giaccherini A, Calisi N, Zangari G, Salvietti E, Passaponti M, et al. Investigations on the electrochemical atomic layer growth of Bi_2Se_3 and the surface limited deposition of bismuth at the silver electrode. Materials. 2018; 11: 1426.
17. Qiao Z, Shang W, Zhang X, Wang C. Underpotential deposition of tin(II) on a gold disc electrode and determination of tin in a tin plate sample. Anal Bioanal Chem. 2005; 381: 1467-1471.
18. Oviedo OA, Reinaudi L, García SG, Leiva EPM. Underpotential deposition: From fundamentals and theory to applications at the nanoscale. Springer; Switzerland. 2016.
19. Mao BW, Tang J, Randler R. Clustering and anisotropy in monolayer formation under potential control: Sn on Au (111). Langmuir. 2002; 18: 5329-5332.
20. Gregory BW, Suggs DW, Stickney JL. Conditions for the deposition of CdTe by electrochemical atomic layer epitaxy. J Electrochem Soc. 1991; 138: 1279-1284.
21. Mendoza-Huizar LH, Robles J, Palomar-Pardave M. Theoretical and experimental study of cobalt nucleation and growth onto gold substrate with different crystallinity. J Electrochem Soc. 2005; 152: C265-C271.
22. Flowers BH, Wade TL, Garvey JW, Lay M, Happek U, Stickney JL. Atomic layer epitaxy of CdTe using an automated electrochemical thin-layer flow deposition reactor. J Electroanal Chem. 2002; 524: 273-285.
23. Yang J, Zhu W, Gao X, Bao S, Fan X. Electrochemical aspects of the formation of Bi2Te3 thin film via the route of ECALE. J Electroanal Chem. 2005; 577: 117-123.

24. Grujicic D, Pesic B. Electrodeposition of copper: The nucleation mechanisms. Electrochim Acta. 2002; 47: 2901-2912.
25. Shalvoy RB, Fisher GB, Stiles PJ. X-ray photoemission studies of the valence bands of nine IV-VI compounds. Phys Rev B. 1977; 15: 1680-1697.
26. Neudachina VS, Shatalova TB, Shtanov VI, Yashina LV, Zyubina TS, Tamm ME, et al. XPS study of SnTe(1 0 0) oxidation by molecular oxygen. Surf Sci. 2005; 584: 77-82.
27. Sugai S, Murase K, Kawamura H. Carrier density dependence of soft TO-phonon in SnTe by Raman scattering. Solid State Commun. 1977; 23: 127-129.
28. An C, Tang K, Hai B, Shen G, Wang C, Qian Y. Solution-phase synthesis of monodispersed SnTe nanocrystallites at room temperature. Inorganic Chem Commun. 2003; 6: 181-184.
29. Salavati-Niasari M, Bazarganipour M, Davar F, Fazl AA. Simple routes to synthesis and characterization of nanosized tin telluride compounds. Appl Surf Sci. 2010; 257: 781-785.
30. Giaccherini A, Montegrossi G, Di Benedetto F, Innocenti M. Thermochemistry of the E-ALD process for the growth of Cu_xZn_yS on Ag (111): Interpretation of experimental data. Electrochim Acta. 2018; 262: 135-143.
31. Vaidyanathan R, Stickney JL, Cox SM, Compton SP, Happek U. Formation of In_2Se_3 thin films and nanostructures using electrochemical atomic layer epitaxy. J Electroanal Chem. 2003; 559: 55-61.
32. Scharifker B, Hills G. Theoretical and experimental studies of multiple nucleation. Electrochim Acta. 1983; 28: 879-889.